Investigation of Mn and Fe substitution effects on the characteristics of high-voltage $LiCo_{1-x}M_xPO_4$ (x = 0.1, 0.4) cathodes prepared by sol-gel route

Daniele Di Lecce[a], Vincenzo Gancitano[a], and Jusef Hassoun[a,b,*]

[a] *Department of Chemical and Pharmaceutical Sciences, University of Ferrara, Via Fossato di Mortara, 17, 44121, Ferrara, Italy.*

[b] *National Interuniversity Consortium of Materials Science and Technology (INSTM), University of Ferrara Research Unit, University of Ferrara, Via Fossato di Mortara, 17, 44121, Ferrara, Italy.*

*Corresponding author: jusef.hassoun@unife.it

Abstract

Herein we provide a fundamental study revealing the substantial changes promoted by manganese and iron substitution for cobalt in high-voltage $LiCoPO_4$ olivine cathode. Therefore, $LiCoPO_4$, $LiCo_{0.9}Fe_{0.1}PO_4$, $LiCo_{0.6}Fe_{0.4}PO_4$, $LiCo_{0.9}Mn_{0.1}PO_4$ and $LiCo_{0.6}Mn_{0.4}PO_4$ are synthesized by a sol-gel pathway and comparatively investigated in terms of structure, morphology and electrochemical features in lithium battery. Beside the observed effects on structure, particle size and metals distribution, the work reveals a gradually enhancing electrode reaction by increasing the Fe content in $LiCo_{0.9}Fe_{0.1}PO_4$ and $LiCo_{0.6}Fe_{0.4}PO_4$, with Co^{3+}/Co^{2+} and Fe^{3+}/Fe^{2+} signatures at 4.8 and 3.5 V *vs.* Li^+/Li, respectively. On the other hand, the introduction of Mn leads to a progressive electrode deactivation in $LiCo_{0.9}Mn_{0.1}PO_4$ and $LiCo_{0.6}Mn_{0.4}PO_4$ due to an intrinsic hindering of the Mn^{3+}/Mn^{2+} process at 4.1 V *vs.* Li^+/Li. The reasons accounting for such an intriguing behavior are

investigated in detail using electrochemical impedance spectroscopy within the potential range of the redox processes. The study reveals that manganese and iron substitutions in the high-voltage olivine have opposite effects on the charge transfer resistance, *i.e.*, detrimental for the former while beneficial for the latter with remarkable enhancement of the reversible capacity, the coulombic efficiency, and the cycle life. Such results provide to the scientific community useful information on possible strategies to enhance the emerging $LiCoPO_4$ high voltage electrode by transition metal substitution.

Keywords

$LiCoPO_4$; Olivine; Phospho-olivine; $LiMnPO_4$; $LiFePO_4$; Energy density; Lithium-ion batteries; Metal substitution.

Introduction

Lithium-ion batteries are electrochemical energy storage systems mostly employed in widespread portable electronic devices, such as laptops, smartphones and tablets, as well as electric vehicles.[1] Driven by the growing interest in sustainable mobility, a great deal of efforts is now devoted towards the developments of high-energy batteries ensuring long-range electric cars (EVs) with performances matching the ones of vehicles powered by internal combustion engines (ICEs). In this respect, the formulation of advanced cathodes with higher voltage and capacity compared to the state of the art may play a crucial role, and is therefore gaining the attention of the scientific community.[2] Among the various positive electrodes investigated so far,[3] the $LiCoPO_4$ olivine has intriguing electrochemical characteristics, namely a flat working voltage plateau as high as 4.8 V *vs.* Li^+/Li and a theoretical capacity of 167 mAh g^{-1},[4] that is, a value approaching those of high-performance $LiNi_{0.80}Co_{0.15}Al_{0.05}O_2$ (NCA) and $LiNi_{0.33}Co_{0.33}Mn_{0.33}O_2$ (NCM) materials operating

at 3.7 V *vs.* Li^+/Li,[5,6] thereby leading to a theoretical energy density of about 800 Wh kg^{-1}.[7] Despite such promising properties, several major issues affecting the actual performances of $LiCoPO_4$ in lab-scale lithium cells have not yet been addressed, thus hindering a possible application.[8] In particular, $LiCoPO_4$ exhibits fast capacity fading,[9–11] large irreversible capacity,[12] intrinsic sluggish kinetics of the Li^+ insertion process limiting the practical capacity and the rate capability,[8] and undesired parasitic reactions in the cell.[13,14] Extensive researches have been focusing on various strategies to enhance the electrochemical behavior, including carbon-coating[15–19] and metal doping/substitution,[20–22] based on the remarkable achievement obtained for the $LiFePO_4$ olivine since its first report in the late nineties.[23,24] Indeed, the characteristic atom arrangement of the olivine-type framework, in which the transition metal and Li occupy 4c and 4a octahedral sites while P is in tetrahedral coordination, leads to a poor electronic conductivity due to low electron delocalization and allows a one-dimensional Li^+ migration within the [010] channels by nonlinear path.[25,26] Therefore, the electron and Li^+ transport properties are strongly affected by crystal lattice ordering, morphology, and the presence of electronically conductive additives, thus requiring suitable synthesis routes to ensure the proper electrochemical process in lithium cells.[8,27–29] Moreover, the introduction within Co-based phospho-olivines of the Fe^{3+}/Fe^{2+} and Mn^{3+}/Mn^{2+} redox centers reacting at about 3.5 and 4.1 V *vs.* Li^+/Li ($LiCo_{1-x}M_xPO_4$ with M = Fe, Mn) has been explored as a viable approach to improve the performances in terms of Li^+ exchange ability and capacity retention.[30–36] Promising results have shown that the incorporation of Fe^{2+} and Fe^{3+} may affect the concentration of punctual defects in the lattice, such as lithium vacancies and anti-site mixing between the 4a and 4c octahedral sites,[37,38] widen the Li^+ transport channels,[39] and stabilize the Co^{3+}/Co^{2+} couple,[40] while the presence of Mn^{2+} may decrease the particle size and stabilize the electrode surface.[31]

Despite of the several papers reported so far on $LiCo_{1-x}M_xPO_4$ materials (M = Fe, Mn),[30–35,41] most of the work has been focusing on the investigation of the effects of one transition metal, *i.e.*, either manganese or iron. Moreover, the literature results refer to different compounds prepared by various approaches, such as solid-state,[34] solvothermal[31,33] and sol-gel,[36] and tested in diverse conditions. Thus, a comparative evaluation based on the existing literature may be strongly affected by the experimental protocols. Both the Fe and Mn-substituted $LiCoPO_4$ have shown enhanced capacity and cycling stability compared to the pristine compound,[30,31,33,36,41] even though the poor behavior of phospho-olivine cathodes with high manganese ratio has been evidenced in many works.[42] On the other hand, a recent report on the mixed $LiFe_{0.25}Mn_{0.5}Co_{0.25}PO_4$ olivine has shown intrinsic hindering of the Mn^{3+}/Mn^{2+} process with respect to the Co^{3+}/Co^{2+} and Fe^{3+}/Fe^{2+} ones, thereby suggesting that the electrochemical activity is affected by local effects on the redox center besides bulk properties such as the ionic and electronic conductivities.[43] Therefore, a comparative study of pristine $LiCoPO_4$ and phospho-olivine cathodes containing Mn and Fe at various degrees of substitution is strongly required to fully elucidate the intrinsic characteristics of the Co^{3+}/Co^{2+}, Mn^{3+}/Mn^{2+} and Fe^{3+}/Fe^{2+} couples. Such an investigation should be carried out by examining materials with similar microstructural features, since structure and morphology may remarkably affect the electrochemical performances.[29] In this regard, the development of a synthesis route for preparing $LiMPO_4$ compounds suitable for a wide stoichiometry range is crucial. Among the numerous synthetic strategies hitherto proposed,[8] the simple sol-gel pathway is a versatile approach which allows a fine tuning of morphology and particle size, that is, critical properties to ensure fast Li^+ (de)insertion.[44]

Following this trend, our work sheds further light on important effects of iron and manganese through the comparative investigation of several olivine samples prepared by the sol-

gel approach and tested within the same conditions. In particular, we study herein Co-based phospho-olivine materials with increasing concentration of Mn and Fe and evaluate their structural, morphological and Li^+-exchange properties. Therefore, we originally reveal the intrinsic behavior of the metals within the olivine framework in determining the electrode kinetics at various potential *vs.* Li^+/Li by means of a detailed electrochemical impedance spectroscopy study. The investigation is carried out by using X-ray diffraction (XRD), electron microscopies, and electrochemical techniques and involves pristine $LiCoPO_4$, $LiCo_{1-x}Mn_xPO_4$, and $LiCo_{1-x}Fe_xPO_4$, where x is 0.1 and 0.4.

Experimental Section

$LiCo_{1-x}M_xPO_4$ materials with M = Fe, Mn and x = 0, 0.1, 0.4 were prepared by a sol-gel route.[44–46] Lithium dihydrogen phosphate (LiH_2PO_4, 99%, Sigma-Aldrich) was dissolved in 10 ml of water (solution A), while the transition metal acetates (*i.e.*, cobalt(II) acetate tetrahydrate, $Co(CO_2CH_3)_2 \cdot 4H_2O$, ≥98.0%; manganese (II) acetate tetrahydrate, $Mn(CO_2CH_3)_2 \cdot 4H_2O$, ≥99.0%; iron(II) acetate, $Fe(CO_2CH_3)_2$, ≥99.99%, Sigma-Aldrich) and citric acid (≥99.5%, Sigma-Aldrich) were dissolved in 20 ml of water (solution B). Solution A was dropwise added to solution B in order to obtain an aqueous solution containing Li, (Co + M), and citric acid in the molar ratio of 1:1:1, respectively (solution C). Solution C was held at about 60 °C in a silicon oil (Sigma-Aldrich) bath under stirring through a hot plate until formation of a gel (about 12 h). The gel was dried for 12 h at 120 °C under a dry air flow, and then heated at 350 °C with a rate of 2 °C min^{-1}, held at 350 °C for 3 h and naturally cooled to room temperature under an argon flow. The precursor so obtained was ground in an agate mortar, heated at 600 °C with a rate of 2 °C min^{-1}, held at 600 °C for 10 h, heated at 700 °C at 5 °C min^{-1}, held at 700 °C for 3 h and naturally cooled to room temperature

under an argon flow. Afterwards, the precursor was ground in an agate mortar and heated at 850 °C with a rate of 5 °C min^{-1}, held at 850 °C for 3 h and naturally cooled to room temperature under an argon flow. Stoichiometric ratios between the reagents were suitable to obtain $LiCoPO_4$, $LiCo_{0.9}Mn_{0.1}PO_4$, $LiCo_{0.6}Mn_{0.4}PO_4$, $LiCo_{0.9}Fe_{0.1}PO_4$, and $LiCo_{0.6}Fe_{0.4}PO_4$. A further thermal step under an argon flow was performed for the Mn- and Fe-substituted materials in order to get an olivine phases with negligible amount of impurity. Such treatment was carried out by heating the powders from room temperature to 850 °C at 5 °C min^{-1}, holding them at 850°C for 5 h, and cooling naturally down to room temperature. All the thermal steps were carried out in a tubular furnace (GHA 12/300, Carbolite). The materials had a carbon content lower than 5 wt.%.

X-ray diffraction (XRD) patterns of the olivine powders spread on a glass sample holder were collected through a Bruker D8 Advance instrument using a Cu Kα source and a graphite monochromator of the diffracted beam, by performing scans in the 2θ range from 10 to 90° at a rate of 10 s $step^{-1}$ with a step size of 0.02°. Rietveld refinement of the patterns was carried out through the MAUD software,[47] by using the reference parameters of the $LiCoPO_4$ olivine (*Pnma* space group, N. 62, ICSD 291401).[48] The atom occupancies have been fixed to the stoichiometric values, confirmed by energy dispersive X-ray spectroscopy (EDS, see below), and the atomic displacement parameters have been forced to have the same value for Co, Fe, Mn, Li and for the PO_3^- atoms. The weighted-profile (R_{wp}%) and goodness-of-fit (σ) values were ≤ 15 and ≤ 2.0, respectively, for all the samples (see Table 1). Sample morphology was inspected by scanning and transmission electron microscopies (SEM and TEM, respectively) through a Zeiss EVO 40 microscope using and a Zeiss EM 910 microscope using LaB_6 thermionic and tungsten thermionic sources operating at 100 kV, respectively. Sample stoichiometry was confirmed by the EDS analyzer of the former microscope (X-ACT Cambridge Instrument).

Electrodes were prepared by doctor-blade coating on aluminum foils (thickness of 15 μm, MTI Corporation). The electrode slurries were made by mixing the active material, poly(vinylidene fluoride) (PVDF 6020 Solef Solvay), and Super P carbon (Timcal) in the 8:1:1 weight ratio, respectively, in N-methyl-pyrrolidone (Sigma-Aldrich) through an agate mortar. The electrode foils were dried for about 3 h on a hot plate at 70 °C, cut into the form of disks with diameter of 10 mm, and dried overnight at 110 °C under vacuum. The active material loading ranged from 3.6 to 4.1 mg cm^{-2}. A further $LiCo_{0.6}Fe_{0.4}PO_4$ electrode was prepared as above described by using a carbon-cloth current collector (ELAT1400, MTI Corporation) instead of aluminum and cut into the form of a disk with diameter of 14 mm. The electrode using the carbon-cloth support had a $LiCo_{0.6}Fe_{0.4}PO_4$ loading of 7.3 mg cm^{-2}. Two-electrode and three-electrode, Swagelok-type cells[6] were assembled in an Ar-filled glovebox (MBraun, O_2 and H_2O contents lower than 1 ppm) by using the composite electrode as the cathode, lithium-metal disks with diameter of 10 mm as the anode and reference (only for three-electrode cells) electrodes, and a Whatman GF/D as the separator. The cell housing was filled with a 1 M solution of $LiPF_6$ in ethylene carbonate/dimethyl carbonate (EC:DMC 1:1 by volume, battery grade) before sealing the cell inside the glovebox. A 2032 coin-cell (MTI Corporation) was assembled in an Ar-filled glovebox (MBraun, O_2 and H_2O contents lower than 1 ppm) by using the $LiCo_{0.6}Fe_{0.4}PO_4$ electrode on the carbon-cloth substrate, a Gelgard 2400 separator soaked by a 1 M solution of $LiPF_6$ in ethylene carbonate/dimethyl carbonate (EC:DMC 1:1 by volume, battery grade), and a lithium-metal disk with diameter of 14 mm.

Cyclic voltammetry was carried out on three-electrode cells through a VersaSTAT MC Princeton Applied Research (PAR, AMETEK) potentiostat by performing scans at 0.1 mV s^{-1} within the potential ranging from 3.0 to 5.1 V *vs.* Li^+/Li for $LiCoPO_4$, $LiCo_{0.9}Mn_{0.1}PO_4$, and

$LiCo_{0.6}Mn_{0.4}PO_4$ and from 2.0 to 5.1 V *vs.* Li^+/Li for $LiCo_{0.9}Fe_{0.1}PO_4$ and $LiCo_{0.6}Fe_{0.4}PO_4$. Cycling tests were carried out on two-electrode cells by charging with a constant current-constant voltage (CC-CV) procedure and discharging at CC through a Maccor Series 4000 battery test system. A constant current of C/10 (1C = 170 mA g^{-1}) and a CV step at 5.1 V with a current limit of C/30 were used. The cells employing $LiCoPO_4$, $LiCo_{0.9}Mn_{0.1}PO_4$, and $LiCo_{0.6}Mn_{0.4}PO_4$ were cycled within the voltage ranging from 3.0 to 5.1 V, while those using $LiCo_{0.9}Fe_{0.1}PO_4$ and $LiCo_{0.6}Fe_{0.4}PO_4$ were cycled within the voltage ranging from 2.0 to 5.1 V. Specific capacity and current rate were calculated by assuming a $LiCo_{1-x}M_xPO_4$ content in the electrodes of 80 wt.%. Electrochemical impedance spectroscopy (EIS) measurements were carried out on three-electrode cells at several states of charge obtained by means of the CC-CV cycling procedure above described. EIS was performed by applying to the cell an alternate voltage signal having an amplitude of 10 mV and frequency decreasing from 500 kHz to 20 mHz. The CC-CV-EIS experiments were carried out through a VersaSTAT MC Princeton Applied Research (PAR, AMETEK) multichannel potentiostat. The impedance datasets were analyzed by a nonlinear least squares (NLLS) procedure through the Boukamp package.[49] All the electrochemical measurements were performed at 25 °C.

Results and Discussion

Crystal structure is determined by powder diffraction and by Rietveld refinement of the corresponding diffractograms. The XRD patterns of Fig. 1 confirm the single-phase olivine structure (*Pnma* space group, table N. 62) for all the materials and suggest absence of whether significant impurities or nucleation of pristine $LiCoPO_4$, $LiMnPO_4$, and $LiFePO_4$ in the metal-substituted compounds. Rietveld refinement reveals the lattice characteristics, which are affected

by the sample stoichiometry. Indeed, the results in terms of unit cell parameters and volume (Table 1) show a gradual expansion due to substitution of Fe for Co in $LiCo_{0.9}Fe_{0.1}PO_4$ and $LiCo_{0.6}Fe_{0.4}PO_4$ in agreement with the Vegard's relation and with literature reports,[33] although a concurrent decrease of the *c* distance indicates a slight distortion of the cell. It is worth mentioning that similar anisotropic cell expansion in $LiCo_{1-x}Fe_xPO_4$ solid solutions has been already observed and partly attributed to an increase of the M – O distance by raising the Fe/(Fe+Co) ratio.[38,39]

Sample	a/Å	b/Å	c/Å	V/Å ^{3}	GOF (σ)	R_{wp}%
$LiCoPO_4$	10.2062(7)	5.9274(4)	4.7031(4)	284.52(6)	1.8	13
$LiCo_{0.9}Mn_{0.1}PO_4$	10.2294(3)	5.9436(2)	4.7056(2)	286.10(3)	1.8	14
$LiCo_{0.6}Mn_{0.4}PO_4$	10.2035(4)	5.9257(2)	4.7018(2)	284.28(3)	2.0	15
$LiCo_{0.9}Fe_{0.1}PO_4$	10.2141(2)	5.9315(1)	4.6998(1)	284.74(2)	1.6	14
$LiCo_{0.6}Fe_{0.4}PO_4$	10.2506(3)	5.9569(1)	4.6979(1)	286.86(2)	1.9	15

Table 1. Results of Rietveld refinement in terms of lattice parameters, unit cell volume, good-of-fit parameter (GOF), and weighted-profile R factor (R_{wp}%). *Pnma* space group, N. 62.

On the other hand, the Mn-substitution leads to the expected increase of all the lattice parameters in $LiCo_{0.9}Mn_{0.1}PO_4$, while the $LiCo_{0.6}Mn_{0.4}PO_4$ sample is characterized by a shrinkage of the crystal with respect to the pristine $LiCoPO_4$ which cannot be explained by a change of the ionic radius of M^{2+} in the octahedral coordination.[50] Such a contraction might be associated with a drop of punctual lattice defects, such as the mixing between lithium and transition metal ions occupying the octahedral 4a and 4c sites, respectively, which is typically promoted by high-temperature annealing.[33,51,52] In this respect, it is noteworthy that the metal-substituted compounds have been prepared by performing a further thermal treatment with respect to pristine $LiCoPO_4$ in

order to get a pure olivine phase, as revealed by the XRD patterns of Fig. S1 of the Supporting Information. The figure shows minor impurities in the powders after the annealing for 3 h at 850 °C, which are not observed in pristine $LiCoPO_4$. However, an additional heating at 850 °C for 5 h leads to a significant improvement of the sample purity, thereby suggesting that the stoichiometry may affect the kinetics of the phase formation (see the Experimental Section for further details about the synthesis recipe).

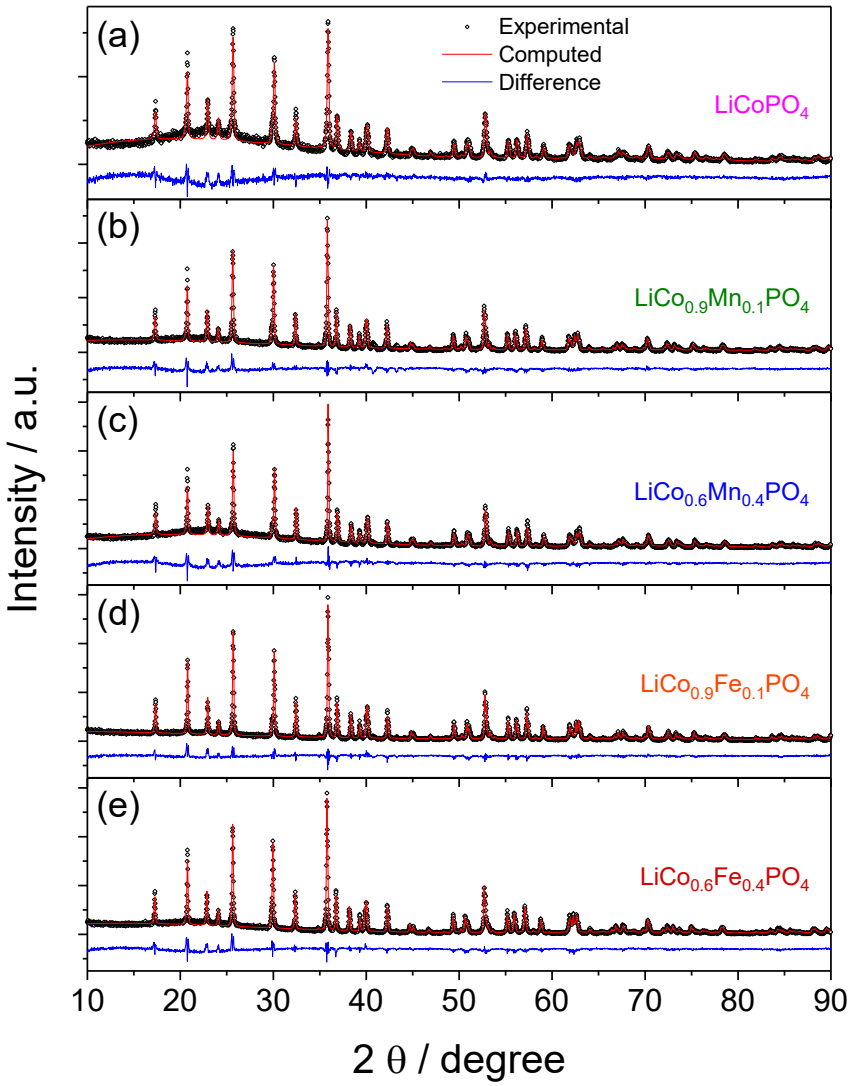

Figure 1. Rietveld refinement of the XRD patterns (*Pnma* space group, N. 62) of **(a)** $LiCoPO_4$, **(b)** $LiCo_{0.9}Mn_{0.1}PO_4$, **(c)** $LiCo_{0.6}Mn_{0.4}PO_4$, **(d)** $LiCo_{0.9}Fe_{0.1}PO_4$, and **(e)** $LiCo_{0.6}Fe_{0.4}PO_4$. In detail: experimental (black dots) and calculated (red line) patterns, difference profile (blue line).

Crystal lattice ordering and presence of anti-site defects between transition metal and lithium may play a crucial role for ensuring fast Li^+ transport within the [010] channels of phospho-olivine cathodes.[51] However, it is worth mentioning that post-synthesis heat treatments typically cause an increase of the crystallite size,[8] which has an adverse effect on the Li^+-exchange ability of olivine compounds,[53] although they may actually decrease the concentration of punctual defects in the ionic framework, as already mentioned.[33,51,52] Therefore, a suitable compromise in terms of synthesis conditions is required to limit an excessive particle growth, leading to an increase of the Li^+ and electron path lengths, and mitigate the presence of anti-site cation mixing which may hinder the one-dimensional (de)lithiation in $LiCo_{1-x}M_xPO_4$ materials (M = Fe, Mn and $0 \leq x \leq 1$).[12,54] Furthermore, nanometric particle size may promote undesired electrolyte decomposition at high voltage *vs.* Li^+/Li,[8,55] thus causing a gradual increase of the electrode/electrolyte interphase resistance during cycling,[56] and decrease the electrode tap density with negative effects on the volumetric energy densities.[8]

The morphological features of the materials have been herein investigated by SEM and TEM. Fig. 2, showing the related micrographs as well as the EDS maps, reveals that the samples are formed by micrometric aggregates of particles ranging from few hundreds of nanometers to several microns and suggests homogenous distribution of the various elements, in agreement with the single olivine phase observed by XRD. Elemental analyses by EDS confirm the stoichiometry for all the materials. Furthermore, the primary particles of all samples have a prismatic-like shape with smoothed edges, as already reported for similar phospho-olivine powders.[57] Therefore, the

results of XRD and electron microscopies as well as the above reported considerations suggest a suitable combination of structural and morphological characteristics for electrochemical Li^+ (de)insertion in lithium cell.

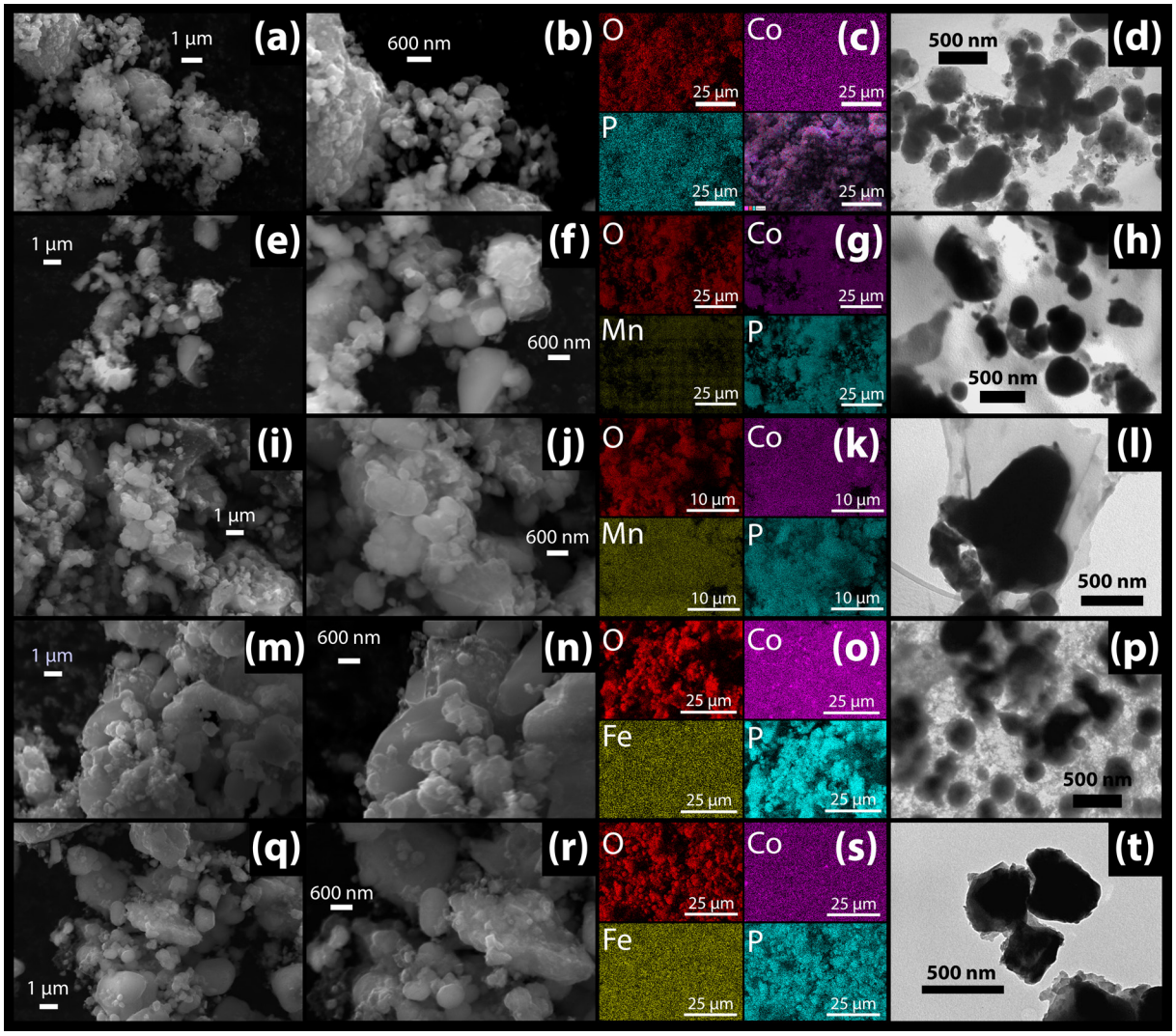

Figure 2. Electron microscopy analyses of **(a-d)** $LiCoPO_4$, **(e-h)** $LiCo_{0.9}Mn_{0.1}PO_4$, **(i-l)** $LiCo_{0.6}Mn_{0.4}PO_4$, **(m-p)** $LiCo_{0.9}Fe_{0.1}PO_4$, and **(q-t)** $LiCo_{0.6}Fe_{0.4}PO_4$. In detail: **(a-b**, **e-f**, **i-j**, **m-n**, **q-r)** SEM images at two different magnifications; **(c**, **g**, **k**, **o**, **s)** SEM-EDS elemental maps of O, Co, P, Mn, and Fe; **(d**, **h** ,**l**, **p**, **t)** TEM images.

Accordingly, the cyclic voltammetry responses shown in Fig. 3 reveal the electrochemical signatures of the Co^{3+}/Co^{2+} and Fe^{3+}/Fe^{2+} redox couples in the olivine framework, while suggest negligible activity due to the Mn^{3+}/Mn^{2+} process. In detail, the first cycle of $LiCoPO_4$ (Fig. 3a) is characterized by two peaks at about 4.9 and 5.0 V *vs.* Li^+/Li during charge, as well as a shoulder followed by a strong peak at about 4.7 *vs.* Li^+/Li during discharge, attributed to the reversible, two-step, biphasic exchange of Li^+ in the olivine lattice with formation of $Li_{2/3}CoPO_4$ and $CoPO_4$ by increasing the potential and restore of $LiCoPO_4$ by lowering back the potential.[58–60] The second and third cycles show a decrease of polarization during both the oxidation and the reduction scans, with formation of $Li_{2/3}CoPO_4$ and $CoPO_4$ occurring at about 4.8 and 4.9 V *vs.* Li^+/Li and the reversed processes centered at about 4.7 V *vs.* Li^+/Li (see Fig. 3a). Such a peak shift suggests a favorable electrode/electrolyte interphase upon cycling.

The voltammetry of $LiCo_{0.9}Mn_{0.1}PO_4$ (Fig. 3b) is characterized by a shoulder at about 4.8 V *vs.* Li^+/Li and a peak at 5.0 V *vs.* Li^+/Li during the first charge, which are reflected into a first-discharge peak at 4.6 V *vs.* Li^+/Li. The subsequent cycles show lower current values compared to the first one, with charge and discharge mostly occurring at 4.9 and 4.6 V *vs.* Li^+/Li, respectively. The CV peaks observed for $LiCo_{0.9}Mn_{0.1}PO_4$ are reasonably attributed to the electrochemical activity of the Co^{3+}/Co^{2+} redox couple[4] as well as to electrolyte decomposition at high potential,[8] without relevant signature in the potential region expected for the Mn^{3+}/Mn^{2+} couple in the phospho-olivine framework, that is, around 4.1 V *vs.* Li^+/Li.[42] The increase of the Mn/(Mn+Co) ratio in $LiCo_{0.6}Mn_{0.4}PO_4$ adversely affects the electrochemical response of the electrode, leading to significantly lower current values upon both charge and discharge compared to $LiCo_{0.9}Mn_{0.1}PO_4$, and noisy profiles. Thus, the first cycle is characterized by an oxidation peak at 4.9 V *vs.* Li^+/Li, similarly to $LiCo_{0.9}Mn_{0.1}PO_4$, while the subsequent scans reveal a reduction

centered at 4.6 V *vs.* Li^+/Li and oxidation occurring through a broad current wave between 4.6 and 5.1 V *vs.* Li^+/Li. Therefore, the Mn^{3+}/Mn^{2+} couple in $LiCo_{1-x}Mn_xPO_4$ compounds apparently has much slower kinetics compared to the Co^{3+}/Co^{2+} one, and hinders the electrochemical activity of the material. The widely-observed poor behavior of Mn-containing phospho-olivines[42] may be attributed in part to the low electronic conductivity[21] and Li^+ diffusion coefficient[27] within the homogenous olivine framework, and in part to the Jahn-Teller distortion around Mn^{3+} hindering the oxidation of Mn^{2+},[61] as already observed in literature for $LiCo_{1-x-y}Mn_xFe_yPO_4$ materials.[43]

The lattice distortion of the $Mn^{3+}O_6$ octahedra in $Mn_{1-x}M_xPO_4$ (where M is a transition metal) has been widely described by means of X-ray/neutron diffraction, X-ray absorption spectroscopy (XAS) and density functional theory (DFT), and associated with the sluggish kinetics of Mn-based phospho-olivines at low x values.[62–64] In detail, a significant increase of the Mn^{3+}–O3′ distance as well as a shrinkage of the Mn^{3+}–O3 bond, both along the equatorial plane of the $Mn^{3+}O_6$ octahedra, occurs together with a slight shortening of the distance between Mn^{3+} and the axial oxygen atoms (O1 and O2; see Fig. S2 in the Supporting Information).[62,63] This geometrical change differs from a strict Jahn-Teller deformation, where the axial bonds stretch and the equatorial bonds shrink, and is therefore called *pseudo* Jahn-Teller distortion.[63] The Jahn-Teller effect accounts for (i) a high formation energy for the hole-polaron Li^+-vacancy complex as well as a high activation energy for its migration,[65,66] and (ii) a mismatch at the interphase between the lithiated and delithiated lattices,[67] thereby hindering the electrochemical reaction in the cell. Our results on $LiCo_{1-x}Mn_xPO_4$ (x = 0.1, 0.4) are in agreement with these observations, although literature works suggested suitable electrode behavior for $x < 0.8$.[30,31]

The first voltammetry cycle of $LiCo_{0.9}Fe_{0.1}PO_4$ (Fig. 3d) is characterized by peaks at 5.0 V *vs.* Li^+/Li during charge and at 4.6 V *vs.* Li^+/Li during discharge, both attributed to the

electrochemical processes of the Co^{3+}/Co^{2+} redox centers.[4] The subsequent cycles show a shoulder at 4.8 V *vs.* Li^+/Li and a peak at 4.9 V *vs.* Li^+/Li during charge, which suggest again a two-step biphasic process[58–60] occurring with lower polarization compared to the first cycle due to the above mentioned formation of favorable electrode/electrolyte interphase, as well as a peak at 4.7 V *vs.* Li^+/Li during discharge. Analogously to $LiCoPO_4$, the presence of two signals around 4.8 V *vs.* Li^+/Li in the CV curves of $LiCo_{0.9}Fe_{0.1}PO_4$ suggests a different (de)lithiation pathway compared to $LiMnPO_4$ and $LiFePO_4$, which has been demonstrated in literature for Co-based olivines by coupling electrochemical and *in situ* XRD measurements.[58–60] Similar behavior has been indeed observed in $LiCo_{1-x}Fe_xPO_4$ materials with low substitution degree ($x < 0.5$),[39] although further work is certainly needed to characterize the phase diagram of cobalt-containing olivines at several compositions in terms of lithium-exchange degree and iron content. It is worth noting that the $LiCo_{0.9}Fe_{0.1}PO_4$ compound herein studied does not exhibit the electrochemical signal of Fe^{3+}/Fe^{2+} at about 3.5 V *vs.* Li^+/Li,[23] which is in agreement with previous reports.[22,33,38–40,68] On the other hand, the increase of the Fe/(Fe+Co) ratio in $LiCo_{0.6}Fe_{0.4}PO_4$ is reflected in the two detectable signatures of the Fe^{3+}/Fe^{2+} and Co^{3+}/Co^{2+} redox couples, occurring at about 3.5[23] and 4.8[4] V *vs.* Li^+/Li, respectively (see Fig. 3e). Indeed, the first cycle shows two oxidation peaks at about 3.6 and 5.0 V *vs.* Li^+/Li, reversed into reduction peaks at about 3.4 and 4.7 V *vs.* Li^+/Li. The subsequent scans reveal a shift of the oxidation process of Co^{2+} to Co^{3+} to about 4.8 V *vs.* Li^+/Li due to the improvement of the electrode/electrolyte interphase, while the other peaks occur without significant changes compared to the first scan.

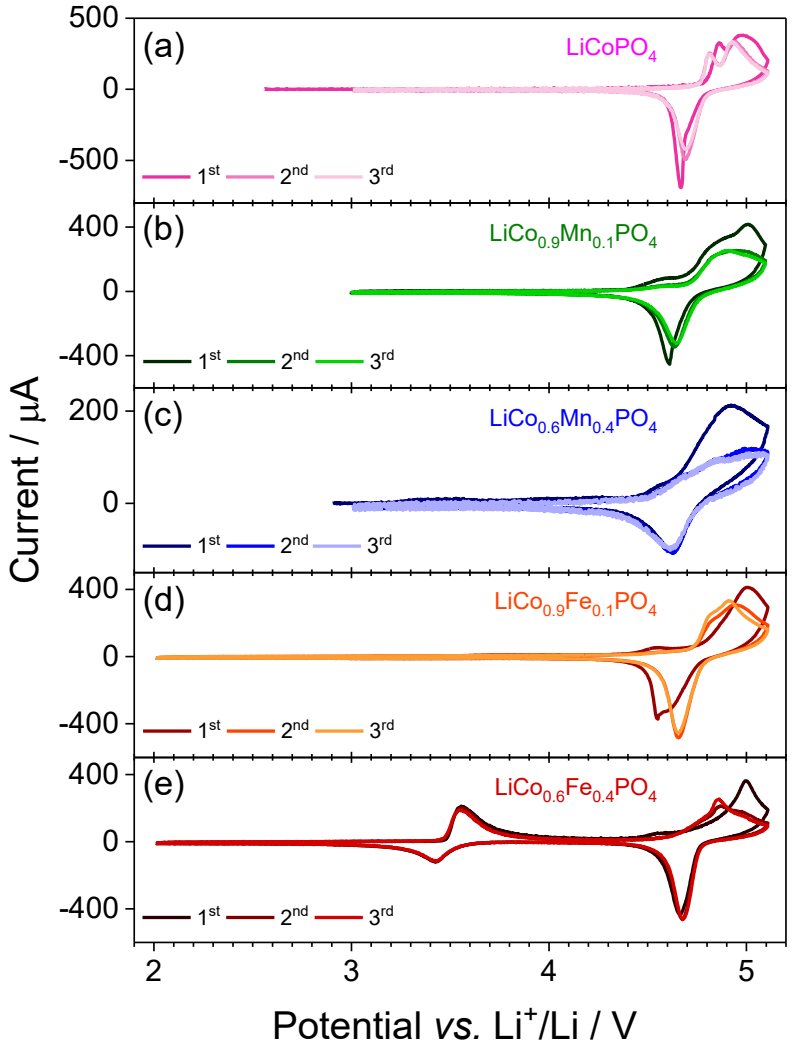

Figure 3. Cyclic voltammetry of **(a)** $LiCoPO_4$, **(b)** $LiCo_{0.9}Mn_{0.1}PO_4$, **(c)** $LiCo_{0.6}Mn_{0.4}PO_4$, **(d)** $LiCo_{0.9}Fe_{0.1}PO_4$, and **(e)** $LiCo_{0.6}Fe_{0.4}PO_4$ in three-electrode cells using lithium-metal counter and reference electrodes at a scan rate of 0.1 mV s^{-1} within potential ranges of 3.0 – 5.1 V *vs.* Li^+/Li (for $LiCoPO_4$, $LiCo_{0.9}Mn_{0.1}PO_4$ and $LiCo_{0.6}Mn_{0.4}PO_4$) and 2.0 – 5.1 V *vs.* Li^+/Li (for $LiCo_{0.9}Fe_{0.1}PO_4$ and $LiCo_{0.6}Fe_{0.4}PO_4$). Electrolyte: 1M $LiPF_6$ in EC:DMC 1:1 by volume. Temperature: 25 °C.

In summary, the different characteristics of Co^{3+}/Co^{2+}, Mn^{3+}/Mn^{2+}, and Fe^{3+}/Fe^{2+} redox centers,[8,24,42] intrinsic bulk properties such as the electronic conductivity[21] and the Li^+ transport

properties,[27] the local Jahn-Teller distortion around Mn^{+3},[61] as well as material characteristics depending on the synthesis conditions, *e.g.*, crystal features and morphology,[8,69] may account for the worst performances in lithium cell of $LiCo_{0.9}Mn_{0.1}PO_4$ and $LiCo_{0.6}Mn_{0.4}PO_4$, and the better behavior of $LiCo_{0.9}Fe_{0.1}PO_4$ and $LiCo_{0.6}Fe_{0.4}PO_4$ compared to $LiCoPO_4$. In addition, the substitutions of manganese and iron for cobalt lead to a slight shift of the Co^{3+}/Co^{2+} potential towards lower values due to a decrease of the ionic character of the Co–O bond.[70] These observations are well confirmed by Fig. 4 which shows the galvanostatic response of the electrodes at C/10 (1C = 170 mAh g^{-1}) in terms of voltage profiles (panels a-e) and cycling behavior (panels f-j). Thus, the first charge of $LiCoPO_4$ evolves through two subsequent plateaus at 4.8 and 4.9 V leading to a capacity of 161 mAh g^{-1} after the CV step (see Fig. 4a and the Experimental Section for details about the testing protocol), while the subsequent discharge reveals a flat plateau centered at 4.7 V and a reversible capacity of 94 mAh g^{-1} (*i.e.*, about 55% of the theoretical capacity). The large irreversible capacity upon the first cycle leading to a coulombic efficiency as low as 58% might be reasonably related to the high working voltage of $LiCoPO_4$, which approaches the oxidation potential of the conventional electrolyte solutions,[8] as well as to possible electrical insulation of the de-lithiated $CoPO_4$. The subsequent cycles are characterized by similar voltage profiles (see Fig. 4a); however, the reversible capacity gradually decreases to 47 mAh g^{-1} after 20 cycles, while the columbic efficiency increases to values ranging from 82 and 86% (see Fig. 4f). The fast capacity fading and the low coulombic efficiency of $LiCoPO_4$ cathodes, as well as remarkable self-discharge, are currently among the main issues hindering a possible application,[8,13] although they have been partially addressed by carbon coating and metal doping/substitution.[15–22]

The worsening of the electrochemical performances owing to the Mn substitution, revealed by panels b-c and g-h of Fig. 4, consists with the voltammetry results of Fig. 3. Indeed, $LiCo_{0.9}Mn_{0.1}PO_4$ exhibits voltage plateaus at about 4.8 and 4.7 V during charge and discharge, respectively, as well as a large inefficiency of the first cycle which significantly decreases in the following cycles along with a slight drop of cell polarization (see Fig. 4b). The material delivers an initial reversible capacity of 80 mAh g^{-1} which gradually falls to 33 mAh g^{-1} after 20 cycles, as shown in Fig. 4g. The $LiCo_{0.6}Mn_{0.4}PO_4$ electrode is characterized by an even poorer behavior with respect to $LiCo_{0.6}Mn_{0.4}PO_4$, both in terms of reversible capacity and coulombic efficiency, due to the above discussed adverse effect of the Mn substitution (see panels c and h of Fig. 4). Moreover, the voltage curves of Fig. 4c exhibit an inflection at about 4.1 V during discharge possibly ascribed to a minor electrochemical activity of the Mn^{3+}/Mn^{2+} couple[42], which was not clearly detected by cyclic voltammetry. On the other hand, the Fe substitution demonstrates a beneficial effect on the cell performance, as indicated by panels d-e and i-j of Fig. 4. $LiCo_{0.9}Fe_{0.1}PO_4$ delivers an initial capacity of 107 mAh g^{-1} through flat plateaus at 4.9 and 4.7 V during charge and discharge, respectively, and exhibits an inflection point around 3.5 V during discharge due to minor reaction of Fe^{3+} (see Fig. 4d). The capacity retention of $LiCo_{0.9}Fe_{0.1}PO_4$ after 20 cycles slightly improves with respect to $LiCoPO_4$, namely, from 50% to 64%, and the coulombic efficiency after the first cycle ranges between 79 and 87%.

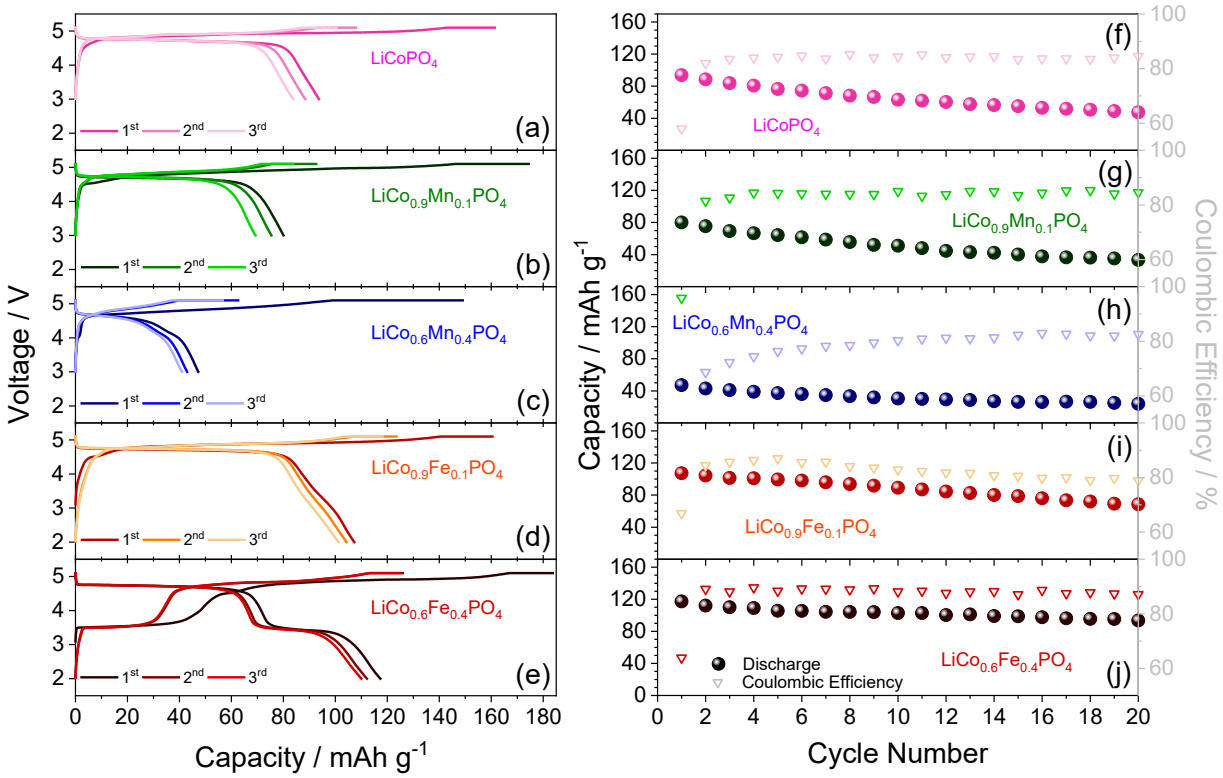

Figure 4. Cycling responses of **(a**, **f)** $LiCoPO_4$, **(b**, **g)** $LiCo_{0.9}Mn_{0.1}PO_4$, **(c**, **h)** $LiCo_{0.6}Mn_{0.4}PO_4$, **(d**, **i)** $LiCo_{0.9}Fe_{0.1}PO_4$, and **(e**, **j)** $LiCo_{0.6}Fe_{0.4}PO_4$ in two-electrode lithium cells in terms of **(a-e)** voltage profiles of the first 3 cycles and **(f-j)** discharge capacity trend with coulombic efficiency (right y-axis). Cells cycled through a constant current (CC) of C/10 (1C = 170 mA g^{-1}) with a constant voltage (CV) step at 5.1 V during charge and a current limit of C/30. Electrolyte: 1M $LiPF_6$ in EC:DMC 1:1 by volume. Temperature: 25 °C.

The $LiCo_{0.6}Fe_{0.4}PO_4$ electrode exchanges Li^+ ions by two voltage plateaus reported in Fig. 4e, attributed to the Fe^{3+}/Fe^{2+} and Co^{3+}/Co^{2+} couples occurring at about 3.5 V and 4.8 V, respectively, which are in full agreement with the CV results (compare Fig. 4e and Fig. 3e). Furthermore, the material reveals a significant improvement of the reversible capacity and the cycling behavior with respect to the other electrodes discussed above. Indeed, $LiCo_{0.6}Fe_{0.4}PO_4$ initially delivers a specific capacity as high as 120 mAh g^{-1}, with a retention of about 80% after

20 cycles, and coulombic efficiency ranging within 87 and 90% after the first cycle (see Fig. 4j). Interestingly, the large inefficiency during the first cycle involves both the low and the high voltage plateaus, as clearly indicated by panel e of Fig. 4, thereby confirming possible effects of the insulation of the delithiated compound in addition to electrolyte decomposition at about 5 V.

The Nyquist plots of EIS measurements reported in Fig. 5 reveal the evolution of the electrode/electrolyte interphase during the first cycle in three-electrode cells. Impedance spectra have been recorded at several states of charge, as indicated in panels a-e of Fig. S3 in the Supporting Information, and analyzed by a NLLS method,[49] which suggested different electrode characteristics at various potential values. Such a study has allowed us to identify equivalent circuits composed of resistance and pseudo-capacitance elements arranged as reported in Table 2 and in Fig. S3f inset of the Supporting Information, which simulate the cell behavior with a high confidence level for most spectra, as shown by the χ^2 values of Table 2 as well as by a good correspondence between the experimental and simulated Nyquist plots (Fig. 5). Even though several phenomena occurring in the cell as a result of the applied voltage signal may account for the observed response and affect the charge transport kinetics,[56] we may clearly distinguish two major interphase resistance components based on the NLLS analysis. Thus, EIS suggests a high-frequency resistance attributed to the electrolyte (R_e), middle-high-frequency pseudo-capacitance and resistance arranged in parallel (Q_i and R_i, respectively) ascribed to the film formed over the electrode surface, middle-low-frequency pseudo-capacitance and resistance arranged in parallel (Q_{dl} and R_{ct}, respectively) reflecting the double layer and the charge transfer, as well as a low frequency pseudo-capacitance associated either with the Warburg-type Li^+ diffusion or with the cell capacitance, depending on the state of charge[56] (a more detailed explanation of the equivalent circuits is provided in the Supporting Information, discussion of Fig. S3).

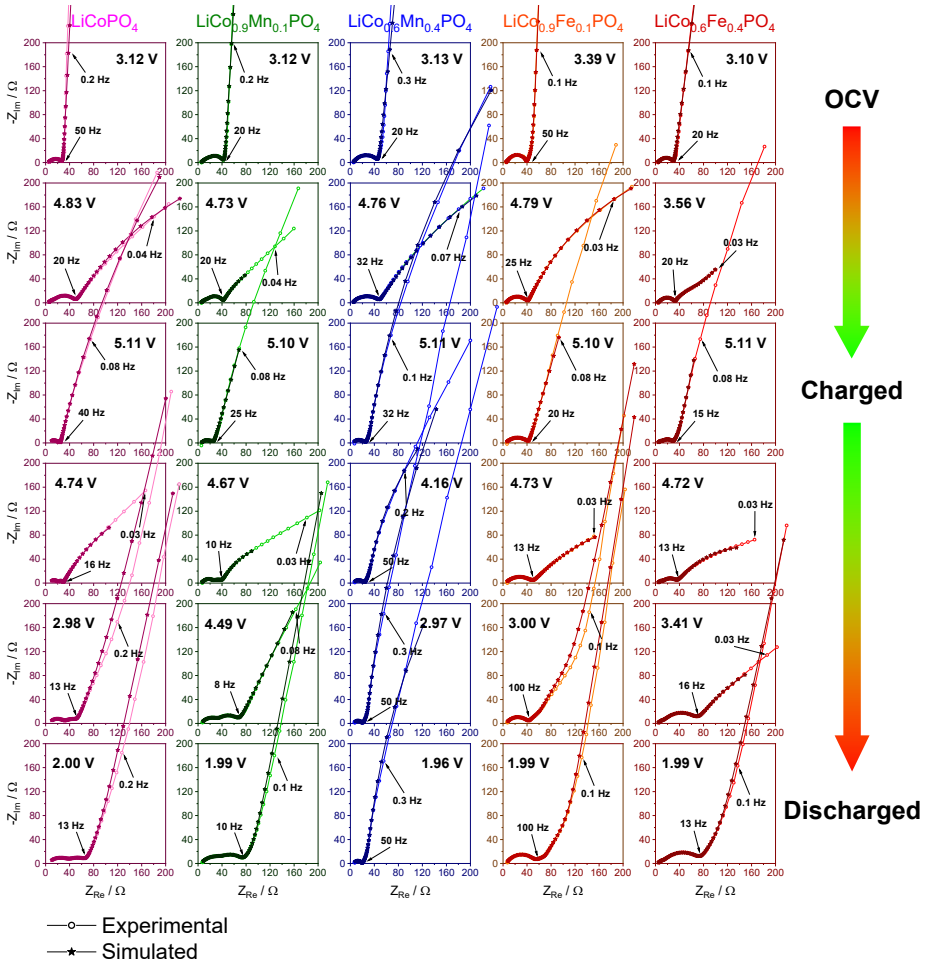

Figure 5. Nyquist plots of EIS measurements at various states of charge with NLLS analysis[49] for $LiCoPO_4$, $LiCo_{0.9}Mn_{0.1}PO_4$, $LiCo_{0.6}Mn_{0.4}PO_4$, $LiCo_{0.9}Fe_{0.1}PO_4$, and $LiCo_{0.6}Fe_{0.4}PO_4$ in three-electrode cells using lithium-metal counter and reference electrodes. The cells have been cycled through a constant current (CC) of C/10 (1C = 170 mA g^{-1}) with a constant voltage (CV) step at 5.1 V during charge and a current limit of C/30. The state of charge is indicated in each panel as the potential *vs.* Li^+/Li obtained by cycling. Electrolyte: 1M $LiPF_6$ in EC:DMC 1:1 by volume. See the related results of NLLS analysis in terms of equivalent circuit, χ^2, resistance of the passivation film ($R_{\Sigma i}$), and charge transfer resistance (R_{ct}) in Table 2 as well as the related voltage profiles of the cycling measurements, equivalent circuit representation and R_{ct} trend in Fig. S3 of the Supporting Information. Temperature: 25 °C.

The Nyquist plots of Fig. 5 show comparable EIS behavior for the electrodes at the various states of charge, namely (i) a blocking-electrode cell response at the OCV, charged and discharged conditions, characterized by high-middle-frequency semicircles and an almost vertical line at low-frequency, and (ii) a response reflecting the low-middle-frequency charge transfer (additional semicircle) and the low-frequency Warburg diffusion at potential values corresponding to the plateaus of Fig. S3a-e.[56]

Table 2 reports the results of the NLLS analysis in terms film and charge transfer resistances at various states of charge. A plot of the latter resistance for all the materials by changing the cell condition is also shown in panel f of Fig. S3 in the Supporting Information. The solid electrode interphase (SEI) film resistance is comparable for all the materials and exhibits slight changes at various states of charge reflecting the expected evolution upon the electrochemical process (see Table 1).[71] On the other hand, the charge transfer resistance is strongly related to both state of charge and material. In particular, the interphase of $LiCo_{0.6}Mn_{0.4}PO_4$ is characterized by a high charge transfer resistance (of the order of 1 kΩ), in agreement with the poor behavior, while much lower values are observed for $LiCo_{0.6}Fe_{0.4}PO_4$, exhibiting the highest reversible capacity by cycling (see Fig. 4). The charge transfer resistance of $LiCoPO_4$ and $LiCo_{0.9}Fe_{0.1}PO_4$ are consistent with the cycling response too, revealing a slight improvement for the latter material, while the relatively low values of $LiCo_{0.9}Mn_{0.1}PO_4$ partially contradicts the poor performance observed by cycling, thus possibly suggesting an electrochemical process hindered by intrinsic limits associated with the structure and the metals ratio in the latter material, rather than by the interphase characteristics. Furthermore, it is worth mentioning that the actual cell behavior during the galvanostatic measurement (Fig. 4) takes into account the average resistance throughout the whole charge and discharge processes.

$LiCoPO_4$	SoC	Eq. Circuit	χ^2	$R_{\sum i}$ (Ω)	R_{ct} (Ω)
	OCV (3.12 V)	R(RQ)Q	3×10^{-4}	4.43 ± 0.09	
	Ch. (4.83 V)	R(RQ)(RQ)(RQ)	2×10^{-4}	45 ± 2	830 ± 50
	Ch. (5.11 V)	R(RQ)(RQ)(RQ)	7×10^{-5}	21 ± 2	
	Disch. (4.74 V)	R(RQ)(RQ)(RQ)	7×10^{-5}	25 ± 1	520 ± 30
	Disch. (2.98 V)	R(RQ)(RQ)(RQ)Q	7×10^{-4}	50 ± 8	
	Disch. (2.00 V)	R(RQ)(RQ)(RQ)Q	4×10^{-4}	60 ± 10	
$LiCo_{0.9}Mn_{0.1}PO_4$	SoC	Eq. Circuit	χ^2	$R_{\sum i}$ (Ω)	R_{ct} (Ω)
	OCV (3.12 V)	R(RQ)(RQ)Q	2×10^{-4}	40 ± 4	
	Ch. (4.73 V)	R(RQ)(RQ)(RQ)	6×10^{-5}	36 ± 2	260 ± 20
	Ch. (5.10 V)	R(RQ)(RQ)Q	1×10^{-4}	22 ± 10	
	Disch. (4.67 V)	R(RQ)(RQ)(RQ)	7×10^{-5}	34 ± 1	210 ± 10
	Disch. (4.49 V)	R(RQ)(RQ)Q	1×10^{-4}	63 ± 2	
	Disch. (2.00 V)	R(RQ)(RQ)(RQ)Q	2×10^{-4}	70 ± 10	
$LiCo_{0.6}Mn_{0.4}PO_4$	SoC	Eq. Circuit	χ^2	$R_{\sum i}$ (Ω)	R_{ct} (Ω)
	OCV (3.13 V)	R(RQ)Q	4×10^{-4}	42.8 ± 0.3	
	Ch. (4.76 V)	R(RQ)(RQ)(RQ)	3×10^{-4}	40 ± 10	1100 ± 100
	Ch. (5.11 V)	R(RQ)(RQ)(RQ)(RQ)	4×10^{-5}	30 ± 20	
	Disch. (4.16 V)	R(RQ)(RQ)(RQ)(RQ)	3×10^{-5}	30 ± 20	970 ± 40
	Disch. (2.97 V)	R(RQ)(RQ)(RQ)(RQ)	7×10^{-5}	23 ± 3	
	Disch. (1.96 V)	R(RQ)(RQ)(RQ)	9×10^{-5}	29 ± 3	
$LiCo_{0.9}Fe_{0.1}PO_4$	SoC	Eq. Circuit	χ^2	$R_{\sum i}$ (Ω)	R_{ct} (Ω)
	OCV (3.39 V)	R(RQ)(RQ)(RQ)Q	3×10^{-4}	33 ± 1	
	Ch. (4.79 V)	R(RQ)(RQ)	4×10^{-4}	36.6 ± 0.3	740 ± 40
	Ch. (5.10 V)	R(RQ)Q	2×10^{-4}	39.4 ± 0.2	
	Disch. (4.73 V)	R(RQ)(RQ)	2×10^{-4}	45.6 ± 0.4	450 ± 40
	Disch. (3.00 V)	R(RQ)(RQ)(RQ)Q	1×10^{-3}	39 ± 2	
	Disch. (1.99 V)	R(RQ)(RQ)(RQ)Q	1×10^{-4}	49 ± 1	
$LiCo_{0.6}Fe_{0.4}PO_4$	SoC	Eq. Circuit	χ^2	$R_{\sum i}$ (Ω)	R_{ct} (Ω)
	OCV (3.10 V)	R(RQ)Q	3×10^{-4}	27.2 ± 0.2	
	Ch. (3.56 V)	R(RQ)(RQ)(RQ)Q	3×10^{-5}	27.8 ± 0.8	28 ± 6
	Ch. (5.11 V)	R(RQ)(RQ)(RQ)Q	5×10^{-5}	25.8 ± 0.9	
	Disch. (4.72 V)	R(RQ)(RQ)(RQ)	8×10^{-5}	31.0 ± 0.8	241 ± 7
	Disch. (3.41 V)	R(RQ)(RQ)(RQ)	5×10^{-5}	66 ± 1	430 ± 30
	Disch. (1.99 V)	R(RQ)(RQ)(RQ)Q	2×10^{-4}	73 ± 2	

Table 2. Results of NLLS analysis of EIS data for $LiCoPO_4$, $LiCo_{0.9}Mn_{0.1}PO_4$, $LiCo_{0.6}Mn_{0.4}PO_4$, $LiCo_{0.9}Fe_{0.1}PO_4$, and $LiCo_{0.6}Fe_{0.4}PO_4$ at various states of charge in three-electrode cells using lithium-metal counter and reference electrodes. In detail: state of charge (SoC) determined as potential *vs.* Li^+/Li, equivalent circuit, χ^2, resistance of the passivation film ($R_{\sum i}$, Ω), and charge transfer resistance (R_{ct}, Ω). The cells have been cycled through a constant current (CC) of C/10 (1C = 170 mA g^{-1}) with a constant voltage (CV) step at 5.1 V during charge and a current limit of C/30. Electrolyte: 1M $LiPF_6$ in EC:DMC 1:1 by volume. See the related Nyquist plots, voltage profiles of the cycling measurements, equivalent circuit representation, and R_{ct} trend in Figs. 5 and S3 of the Supporting Information. Further description of the equivalent circuits is provided in the Supporting Information (discussion of Fig. S3). Analysis performed by using the Boukamp software.[49]

Therefore, our results show that the $LiCo_{0.6}Fe_{0.4}PO_4$ material is characterized by the best electrochemical performances, namely the highest reversible capacity and coulombic efficiency along with enhanced electrode/electrolyte interphase. Despite the higher capacity compared to $LiCo_{0.9}Fe_{0.1}PO_4$ and $LiCoPO_4$, the high iron content leads to a lower average working voltage which negatively affects the energy density. On the other hand, the decrease of Co content may suitably enhance the environmental compatibility of the electrode. In this respect, we suggested in a recent work[43] a new olivine compound including iron, manganese and cobalt, *i.e.*, $LiFe_{0.25}Mn_{0.5}Co_{0.25}PO_4$, which ensured promising electrochemical behavior in terms of potential *vs*. Li^+/Li, reversible capacity and cycling behavior. Based on the results reported herein, further work is certainly needed to assess an optimal metal combination possibly including various metals with a high Co ratio.

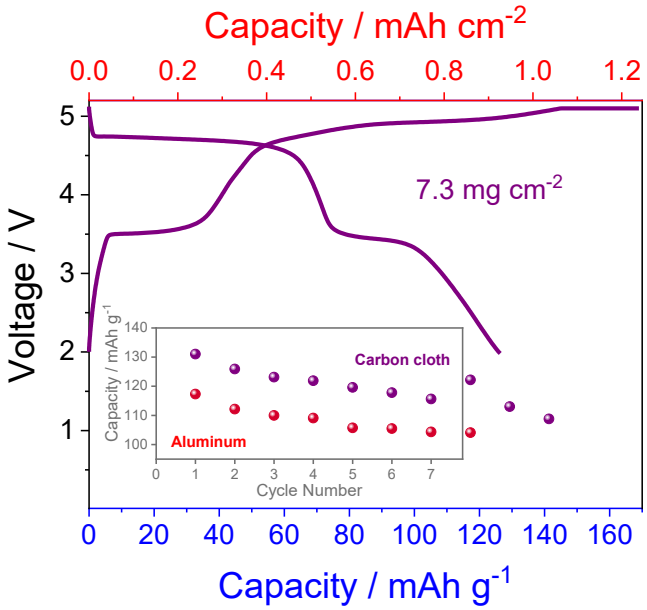

Figure 6. Voltage profile of the second cycle for $LiCo_{0.6}Fe_{0.4}PO_4$ in a lithium cell using a carbon-cloth electrode support instead of conventional aluminum. Bottom x-axis shows the gravimetric capacity (mAh g^{-1}) referred to the cathode (11.3 mg), whereas the top x-axis shows the areal capacity (mAh cm^{-2}) referred to the electrode geometric area (1.54 cm^2). Inset: cycling trend of $LiCo_{0.6}Fe_{0.4}PO_4$ in two lithium cells using the carbon-cloth support and conventional aluminum, respectively. Cells cycled through a constant current (CC) of C/10 (1C = 170 mA g^{-1}) with a constant voltage (CV) step at 5.1 V during charge and a current limit of C/30. Electrolyte: 1M $LiPF_6$ in EC:DMC 1:1 by volume. Temperature: 25 °C. The electrode using the carbon-cloth substrate had an active material loading of 7.3 mg cm^{-2}, while the one employing aluminum contained 3.7 mg cm^{-2}.

The electrochemical performance of $LiCo_{0.6}Fe_{0.4}PO_4$ may be further improved by using a carbon-cloth current collector ensuring enhanced electric contact between the electrode particles and higher active material loading compared to standard aluminum.[54] Fig. 6 reveals an increase of

the first-cycle reversible capacity from about 120 to 130 mAh g^{-1} (*i.e.*, about 78% of the theoretical one) due to the electrode substrate, despite a loading rising from 3.7 to 7.3 mg cm^{-2}. Such a relatively high loading is reflected into an areal capacity of about 0.9 mAh cm^{-2} (top x-axis in Figure 6) without relevant adverse effects on the cycling trend (see Figure 6 inset). It is worth mentioning that most of the Co-based olivine cathodes investigated in literature contained from 1 to 5 mg cm^{-2} of active material,[11,16,19,22,38,39,46,69,72–77] while only a few reports demonstrated promising electrochemical behavior with practical loading values.[70,78] In spite of the beneficial effects, this particular electrode morphology, already described in a recent report,[79] requires a suitable high-voltage electrolyte solution to mitigate the large irreversible capacity promoted by the high porosity and chemical nature of the carbon-based substrate.[54] This point is crucial for the application of Co-based olivine compound in lithium batteries working at 4.8 V.[9,68,72] Therefore, a proper cell configuration in terms of electrode support, separator,[11,80] and electrolyte solution[9,68,72] might actually ensure suitable reversible capacity and coulombic efficiency.

Conclusions

A comparative investigation of Co-based phospho-olivines including either manganese or iron successfully revealed the effect of the transition metal substitution. $LiCo_{1-x}Mn_xPO_4$ and $LiCo_{1-x}Fe_xPO_4$ materials with x = 0, 0.1, 0.4 were synthesized by a versatile sol-gel approach suitable for preparing this class of electrodes with various compositions. XRD showed a single olivine phase characterized by a homogenous distribution of the metals in agreement with the stoichiometry, as confirmed by EDS, and lattice parameters varying according to the sample composition. SEM and TEM indicated micrometric aggregates of primary particles ensuring suitable charge transfer at the electrode/electrolyte interphase. The electrochemical

characterization, performed by combining voltammetry, galvanostatic cycling and electrochemical impedance spectroscopy at various states of charge, suggested an intrinsic hindering of the Mn^{3+}/Mn^{2+} redox process, which was reflected into a negligible activity at about 4.1 *vs.* Li^+/Li and poor performance for the Mn-containing materials. In particular, the charge transfer resistance increased and the reversible capacity decreased with increasing manganese contents. Instead, the iron substitution for cobalt led to improvements of the electrochemical behavior in terms of capacity, coulombic efficiency and capacity retention. The $LiCo_{0.9}Fe_{0.1}PO_4$ material exhibited electrochemical reaction mostly occurring by a flat plateau at about 4.8 V *vs.* Li^+/Li due to the Co^{3+}/Co^{2+} redox couple and a capacity of 107 mAh g^{-1}, while the $LiCo_{0.6}Fe_{0.4}PO_4$ one delivered about 120 mAh g^{-1} through the Fe^{3+}/Fe^{2+} and Co^{3+}/Co^{2+} processes at about 3.5 and 4.8 V *vs.* Li^+/Li. Furthermore, preliminary cycling tests of $LiCo_{0.6}Fe_{0.4}PO_4$ on a carbon-cloth electrode support indicated a reversible areal capacity of 0.9 mAh cm^{-2}, corresponding to 130 mAh g^{-1}. The impedance analysis provided results in agreement with the cycling behavior, thereby evidencing the crucial role of the charge transfer at the electrode/electrolyte interphase within the potential range of the electrochemical reaction. Our study clearly suggested a beneficial effect of iron and a detrimental effect of manganese in $LiCo_{1-x}M_xPO_4$ phospho-olivines, which became more relevant by increasing the transition metal substitution. Therefore, effective approaches to enhance the performances of $LiCoPO_4$ in lithium cells appeared herein to be the proper combination of structural and morphological properties, a partial iron incorporation into the olivine and the optimization of a suitable cell configuration. Our fundamental evaluation of the metal-substituted phospho-olivines with similar microstructures revealed peculiar responses of Co^{3+}/Co^{2+}, Mn^{3+}/Mn^{2+} and Fe^{3+}/Fe^{2+} redox couples within the polyanionic framework of the various materials, thereby possibly leading to a significant impact on the scientific community working in the field.

Acknowledgements

The authors thank University of Ferrara for funding (Fondo di Ateneo per la Ricerca Locale, FAR 2017), and the agreement "Accordo di Collaborazione Quadro 2015" between University of Ferrara (Department of Chemical and Pharmaceutical Sciences) and Sapienza University of Rome (Department of Chemistry).

Supporting Information. XRD patterns of metal-substituted olivine samples after the 1st and 2nd annealing steps at 850 °C, compared with reference bars of $LiCoPO_4$ olivine and XRD patterns of $LiCoPO_4$ after the 1st annealing step at 850 °C. Schematic structure of the MnO_6 octahedron in the $Mn_{1-x}M_xPO_4$ olivine (where M is a transition metal) showing the *pseudo* Jahn-Teller distortion. Galvanostatic voltage profiles of the olivine cathodes in three-electrode cells using lithium-metal counter and reference electrodes with related charge transfer resistance (R_{ct}) at several states of charge as determined by EIS.

References

(1) Di Lecce, D.; Verrelli, R.; Hassoun, J. Lithium-ion batteries for sustainable energy storage: recent advances towards new cell configurations. *Green Chem.* **2017**, *19* (15), 3442–3467.

(2) Andre, D.; Kim, S.; Lamp, P.; Lux, F.; Maglia, F. Future generations of cathode materials : an automotive industry perspective. *J. Mater. Chem. A Mater. energy Sustain.* **2015**, *3*, 6709–6732.

(3) Li, W.; Song, B.; Manthiram, A. High-voltage positive electrode materials for lithium-ion batteries. *Chem. Soc. Rev.* **2017**, *46* (10), 3006–3059.

(4) Amine, K.; Yasuda, H.; Yamachi, M. Olivine $LiCoPO_4$ as 4.8 V Electrode Material for Lithium Batteries. *Electrochem. Solid-State Lett.* **2000**, *3* (4), 178–179.

(5) Agostini, M.; Ulissi, U.; Di Lecce, D.; Ahiara, Y.; Ito, S.; Hassoun, J. A Lithium-Ion Battery based on an Ionic Liquid Electrolyte, Tin-Carbon Nanostructured Anode, and Li_2O-ZrO_2-Coated $Li[Ni_{0.8}Co_{0.15}Al_{0.05}]O_2$ Cathode. *Energy Technol.* **2015**, *3* (6), 632–637.

(6) Di Lecce, D.; Andreotti, P.; Boni, M.; Gasparro, G.; Rizzati, G.; Hwang, J.-Y.; Sun, Y.-K.; Hassoun, J. Multiwalled Carbon Nanotubes Anode in Lithium-Ion Battery with $LiCoO_2$, $Li[Ni_{1/3}Co_{1/3}Mn_{1/3}]O_2$, and $LiFe_{1/4}Mn_{1/2}Co_{1/4}PO_4$ Cathodes. *ACS Sustain. Chem. Eng.* **2018**, *6* (3), 3225–3232.

(7) Hautier, G.; Jain, A.; Ong, S. P.; Kang, B.; Moore, C.; Doe, R.; Ceder, G. Phosphates as Lithium-Ion Battery Cathodes: An Evaluation Based on High-Throughput ab Initio Calculations. *Chem. Mater.* **2011**, *23* (15), 3495–3508.

(8) Zhang, M.; Garcia-Araez, N.; Hector, A. L. Understanding and development of olivine $LiCoPO_4$ cathode materials for lithium-ion batteries. *J. Mater. Chem. A* **2018**, *6* (30), 14483–14517.

(9) Aravindan, V.; Cheah, Y. L.; Ling, W. C.; Madhavi, S. Effect of LiBOB Additive on the Electrochemical Performance of $LiCoPO_4$. *J. Electrochem. Soc.* **2012**, *159* (9), A1435–A1439.

(10) Markevich, E.; Sharabi, R.; Gottlieb, H.; Borgel, V.; Fridman, K.; Salitra, G.; Aurbach, D.; Semrau, G.; Schmidt, M. a.; Schall, N.; Bruenig, C. Reasons for capacity fading of $LiCoPO_4$ cathodes in $LiPF_6$ containing electrolyte solutions. *Electrochem. commun.* **2012**, *15* (1), 22–25.

(11) Sharabi, R.; Markevich, E.; Borgel, V.; Salitra, G.; Gershinsky, G.; Aurbach, D.; Semrau, G.; Schmidt, M. A.; Schall, N.; Stinner, C. Raman study of structural stability of $LiCoPO_4$ cathodes in $LiPF_6$ containing electrolytes. *J. Power Sources* **2012**, *203*, 109–114.

(12) Brutti, S.; Manzi, J.; De Bonis, A.; Di Lecce, D.; Vitucci, F.; Paolone, A.; Trequattrini, F.; Panero, S. Controlled synthesis of $LiCoPO_4$ by a solvo-thermal method at 220°C. *Mater. Lett.* **2015**, *145*, 324–327.

(13) Manzi, J.; Vitucci, F. M.; Paolone, A.; Trequattrini, F.; Di Lecce, D.; Panero, S.; Brutti, S. Analysis of the self-discharge process in LiCoPO 4 electrodes: bulks. *Electrochim. Acta* **2015**, *179*, 604–610.

(14) Manzi, J.; Brutti, S. Surface chemistry on $LiCoPO_4$ electrodes in lithium cells: SEI formation and self-discharge. *Electrochim. Acta* **2016**, *222*, 1839–1846.

(15) Li, H. H.; Jin, J.; Wei, J. P.; Zhou, Z.; Yan, J. Fast synthesis of core-shell $LiCoPO_4$/C nanocomposite via microwave heating and its electrochemical Li intercalation performances. *Electrochem. commun.* **2009**, *11* (1), 95–98.

(16) Doan, T. N. L.; Taniguchi, I. Effect of spray pyrolysis temperature on physical and electrochemical properties of $LiCoPO_4$/C nanocomposites. *Powder Technol.* **2012**, *217*, 574–580.

(17) Oh, S.-M.; Myung, S.-T.; Sun, Y.-K. Olivine $LiCoPO_4$–carbon composite showing high rechargeable capacity. *J. Mater. Chem.* **2012**, *22* (30), 14932–14937.

(18) Wolfenstine, J.; Read, J.; Allen, J. L. Effect of carbon on the electronic conductivity and discharge capacity $LiCoPO_4$. *J. Power Sources* **2007**, *163* (2), 1070–1073.

(19) Ni, J.; Gao, L.; Lu, L. Carbon coated lithium cobalt phosphate for Li-ion batteries: Comparison of three coating techniques. *J. Power Sources* **2013**, *221*, 35–41.

(20) Wang, F.; Yang, J.; NuLi, Y.; Wang, J. Highly promoted electrochemical performance of 5 V $LiCoPO_4$ cathode material by addition of vanadium. *J. Power Sources* **2010**, *195* (19), 6884–6887.

(21) Wolfenstine, J. Electrical conductivity of doped $LiCoPO_4$. *J. Power Sources* **2006**, *158* (2), 1431–1435.

(22) Allen, J. L.; Allen, J. L.; Thompson, T.; Delp, S. A.; Wolfenstine, J.; Jow, T. R. Cr and Si Substituted-$LiCo_{0.9}Fe_{0.1}PO_4$: Structure, full and half Li-ion cell performance. *J. Power Sources* **2016**, *327*, 229–234.

(23) Padhi, A. K. Phospho-olivines as Positive-Electrode Materials for Rechargeable Lithium Batteries. *J. Electrochem. Soc.* **1997**, *144* (4), 1188–1194.

(24) Zaghib, K.; Guerfi, A.; Hovington, P.; Vijh, A.; Trudeau, M.; Mauger, A.; Goodenough, J. B.; Julien, C. M. Review and analysis of nanostructured olivine-based lithium recheargeable batteries: Status and trends. *J. Power Sources* **2013**, *232*, 357–369.

(25) Masquelier, C.; Croguennec, L. Polyanionic (Phosphates, Silicates, Sulfates) Frameworks as Electrode Materials for Rechargeable Li (or Na) Batteries. *Chem. Rev.* **2013**, *113* (8), 6552–6591.

(26) Tealdi, C.; Heath, J.; Islam, M. S. Feeling the strain: enhancing ionic transport in olivine phosphate cathodes for Li- and Na-ion batteries through strain effects. *J. Mater. Chem. A* **2016**, *4* (18), 6998–7004.

(27) Di Lecce, D.; Hassoun, J. Lithium Transport Properties in $LiMn_{1-\alpha}Fe_{\alpha}PO_4$ Olivine Cathodes. *J. Phys. Chem. C* **2015**, *119* (36), 20855–20863.

(28) Kandhasamy, S.; Nallathamby, K.; Minakshi, M. Role of structural defects in olivine cathodes. *Prog. Solid State Chem.* **2012**, *40* (1–2), 1–5.

(29) Ludwig, J.; Nilges, T. Recent progress and developments in lithium cobalt phosphate chemistry- Syntheses, polymorphism and properties. *J. Power Sources* **2018**, *382*, 101–115.

(30) Han, Y. H.; Ni, J. F.; Liu, J. Z.; Wang, H. B.; Gao, L. J. Improving electrochemical

performance of $LiCoPO_4$ via Mn substitution. *Mater. Technol.* **2013**, *28* (5), 265–269.

(31) Ni, J. F.; Han, Y.; Liu, J.; Wang, H.; Gao, L. Improving Electrochemical Properties of $LiCoPO_4$ by Mn Substitution: A Case Research on $LiCo_{0.5}Mn_{0.5}PO_4$. *ECS Electrochem. Lett.* **2012**, *2* (1), A3–A5.

(32) Strobridge, F. C.; Middlemiss, D. S.; Pell, A. J.; Leskes, M.; Clément, R. J.; Pourpoint, F.; Lu, Z.; Hanna, J. V.; Pintacuda, G.; Emsley, L.; Samoson, A.; Grey, C. P. Characterising local environments in high energy density Li-ion battery cathodes: a combined NMR and first principles study of $LiFe_xCo_{1-x}PO_4$. *J. Mater. Chem. A* **2014**, *2* (30), 11948–11957.

(33) Di Lecce, D.; Manzi, J.; Vitucci, F. M.; De Bonis, A.; Panero, S.; Brutti, S. Effect of the iron doping in $LiCoPO_4$ cathode materials for lithium cells. *Electrochim. Acta* **2015**, *185*, 17–27.

(34) Yang, S. M. G.; Aravindan, V.; Cho, W. I.; Chang, D. R.; Kim, H. S.; Lee, Y. S. Realizing the Performance of $LiCoPO_4$ Cathodes by Fe Substitution with Off-Stoichiometry. *J. Electrochem. Soc.* **2012**, *159* (7), A1013–A1018.

(35) Allen, J. L.; Thompson, T.; Sakamoto, J.; Becker, C. R.; Jow, T. R.; Wolfenstine, J. Transport properties of $LiCoPO_4$ and Fe-substituted $LiCoPO_4$. *J. Power Sources* **2014**, *254*, 204–208.

(36) Örnek, A.; Can, M.; Yeşildağ, A. Improving the cycle stability of $LiCoPO_4$ nanocomposites as 4.8V cathode: Stepwise or synchronous surface coating and Mn substitution. *Mater. Charact.* **2016**, *116*, 76–83.

(37) Kang, Y.-M.; Kim, Y.-I.; Oh, M.-W.; Yin, R.-Z.; Lee, Y.; Han, D.-W.; Kwon, H.-S.; Kim, J. H.; Ramanath, G. Structurally stabilized olivine lithium phosphate cathodes with enhanced electrochemical properties through Fe doping. *Energy Environ. Sci.* **2011**, *4* (12),

4978–4983.

(38) Brutti, S.; Manzi, J.; Meggiolaro, D.; Vitucci, F. M.; Trequattrini, F.; Paolone, A.; Palumbo, O. Interplay between local structure and transport properties in iron-doped $LiCoPO_4$ olivines. *J. Mater. Chem. A* **2017**, *5* (27), 14020–14030.

(39) Kosova, N. V.; Podgornova, O. A.; Devyatkina, E. T.; Podugolnikov, V. R.; Petrov, S. A. Effect of Fe^{2+} substitution on the structure and electrochemistry of $LiCoPO_4$ prepared by mechanochemically assisted carbothermal reduction. *J. Mater. Chem. A* **2014**, *2* (48), 20697–20705.

(40) Lapping, J. G.; Delp, S. A.; Allen, J. L.; Allen, J. L.; Freeland, J. W.; Johannes, M. D.; Hu, L.; Tran, D. T.; Jow, T. R.; Cabana, J. Changes in Electronic Structure upon Li Deintercalation from $LiCoPO_4$ Derivatives. *Chem. Mater.* **2018**, *30* (6), 1898–1906.

(41) Allen, J. L.; Jow, T. R.; Wolfenstine, J. Improved cycle life of Fe-substituted $LiCoPO_4$. *J. Power Sources* **2011**, *196* (20), 8656–8661.

(42) Aravindan, V.; Gnanaraj, J.; Lee, Y.-S.; Madhavi, S. $LiMnPO_4$ – A next generation cathode material for lithium-ion batteries. *J. Mater. Chem. A* **2013**, *1* (11), 3518–3539.

(43) Di Lecce, D.; Brescia, R.; Scarpellini, A.; Prato, M.; Hassoun, J. A High Voltage Olivine Cathode for Application in Lithium-Ion Batteries. *ChemSusChem* **2016**, *9* (2), 223–230.

(44) Croce, F.; D' Epifanio, A.; Hassoun, J.; Deptula, A.; Olczac, T.; Scrosati, B. A Novel Concept for the Synthesis of an Improved $LiFePO_4$ Lithium Battery Cathode. *Electrochem. Solid-State Lett.* **2002**, *5* (3), A47–A50.

(45) Di Lecce, D.; Hu, T.; Hassoun, J. Electrochemical features of $LiMnPO_4$ olivine prepared by sol-gel pathway. *J. Alloys Compd.* **2017**, *693*, 730–737.

(46) Ni, J.; Wang, H.; Gao, L.; Lu, L. A high-performance $LiCoPO_4$/C core/shell composite for

Li-ion batteries. *Electrochim. Acta* **2012**, *70*, 349–354.

(47) Lutterotti, L.; Chateigner, D.; Ferrari, S.; Ricote, J. Texture, residual stress and structural analysis of thin films using a combined X-ray analysis. *Thin Solid Films* **2004**, *450* (1), 34–41.

(48) Brutti, S.; Manzi, J.; De Bonis, A.; Di Lecce, D.; Vitucci, F.; Paolone, A.; Trequattrini, F.; Panero, S. Erratum: Controlled synthesis of $LiCoPO_4$ by a solvo-thermal method at 220 °c (Materials Letters (2015) 145 (324-327) DOI 10.1016/j.matlet.2015.01.137). *Mater. Lett.* **2016**, *172*, 98.

(49) Boukamp, B. A. A Nonlinear Least Squares Fit procedure for analysis of immittance data of electrochemical systems. *Solid State Ionics* **1986**, *20* (1), 31–44.

(50) Shannon, R. D. Revised effective ionic radii and systematic studies of interatomic distances in halides and chalcogenides. *Acta Crystallogr. Sect. A* **1976**, *32* (5), 751–767.

(51) Chen, J.; Graetz, J. Study of antisite defects in hydrothermally prepared $LiFePO_4$ by in situ x-ray diffraction. *ACS Appl. Mater. Interfaces* **2011**, *3* (5), 1380–1384.

(52) Chen, J.; Whittingham, M. S. Hydrothermal synthesis of lithium iron phosphate. *Electrochem. commun.* **2006**, *8* (5), 855–858.

(53) Gaberscek, M.; Dominko, R.; Jamnik, J. Is small particle size more important than carbon coating? An example study on $LiFePO_4$ cathodes. *Electrochem. commun.* **2007**, *9* (12), 2778–2783.

(54) Di Lecce, D.; Carbone, L.; Gancitano, V.; Hassoun, J. Rechargeable lithium battery using non-flammable electrolyte based on tetraethylene glycol dimethyl ether and olivine cathodes. *J. Power Sources* **2016**, *334*, 146–153.

(55) Di Lecce, D.; Fasciani, C.; Scrosati, B.; Hassoun, J. A Gel–Polymer Sn–C/$LiMn_{0.5}Fe_{0.5}PO_4$

Battery Using a Fluorine-Free Salt. *ACS Appl. Mater. Interfaces* **2015**, *7* (38), 21198–21207.

(56) Di Lecce, D.; Verrelli, R.; Hassoun, J. New lithium ion batteries exploiting conversion/alloying anode and $LiFe_{0.25}Mn_{0.5}Co_{0.25}PO_4$ olivine cathode. *Electrochim. Acta* **2016**, *220*, 384–390.

(57) Fisher, C. A. J.; Islam, M. S. Surface structures and crystal morphologies of $LiFePO_4$: relevance to electrochemical behaviour. *J. Mater. Chem.* **2008**, *18* (11), 1209–1215.

(58) Bramnik, N. N.; Nikolowski, K.; Baehtz, C.; Bramnik, K. G.; Ehrenberg, H. Phase Transitions Occurring upon Lithium Insertion−Extraction of $LiCoPO_4$. *Chem. Mater.* **2007**, *19* (4), 908–915.

(59) Kaus, M.; Issac, I.; Heinzmann, R.; Doyle, S.; Mangold, S.; Hahn, H.; Chakravadhanula, V. S. K.; Kübel, C.; Ehrenberg, H.; Indris, S. Electrochemical Delithiation/Relithiation of $LiCoPO_4$: A Two-Step Reaction Mechanism Investigated by in Situ X-ray Diffraction, in Situ X-ray Absorption Spectroscopy, and ex Situ $^{7}Li/^{31}P$ NMR Spectroscopy. *J. Phys. Chem. C* **2014**, *118* (31), 17279–17290.

(60) Strobridge, F. C.; Clément, R. J.; Leskes, M.; Middlemiss, D. S.; Borkiewicz, O. J.; Wiaderek, K. M.; Chapman, K. W.; Chupas, P. J.; Grey, C. P. Identifying the Structure of the Intermediate, $Li_{2/3}CoPO_4$, Formed during Electrochemical Cycling of $LiCoPO_4$. *Chem. Mater.* **2014**, *26* (21), 6193–6205.

(61) Yamada, A.; Hosoya, M.; Chung, S. C.; Kudo, Y.; Hinokuma, K.; Liu, K. Y.; Nishi, Y. Olivine-type cathodes: Achievements and problems. *J. Power Sources* **2003**, *119–121*, 232–238.

(62) Yamada, A.; Takei, Y.; Koizumi, H.; Sonoyama, N.; Kanno, R.; Itoh, K.; Yonemura, M.;

Kamiyama, T. Electrochemical, Magnetic, and Structural Investigation of the $Li_x(Mn_yFe_{1-y})PO_4$ Olivine Phases. *Chem. Mater.* **2006**, *18* (3), 804–813.

(63) Piper, L. F. J.; Quackenbush, N. F.; Sallis, S.; Scanlon, D. O.; Watson, G. W.; Nam, K.-W.; Yang, X.-Q.; Smith, K. E.; Omenya, F.; Chernova, N. A.; Whittingham, M. S. Elucidating the Nature of Pseudo Jahn–Teller Distortions in Li_xMnPO_4: Combining Density Functional Theory with Soft and Hard X-ray Spectroscopy. *J. Phys. Chem. C* **2013**, *117* (20), 10383–10396.

(64) Iadecola, A.; Perea, A.; Aldon, L.; Aquilanti, G.; Stievano, L. Li deinsertion mechanism and Jahn–Teller distortion in $LiFe_{0.75}Mn_{0.25}PO_4$: an operando X-ray absorption spectroscopy investigation. *J. Phys. D. Appl. Phys.* **2017**, *50* (14), 144004.

(65) Ong, S. P.; Chevrier, V. L.; Ceder, G. Comparison of small polaron migration and phase separation in olivine $LiMnPO_4$ and $LiFePO_4$ using hybrid density functional theory. *Phys. Rev. B - Condens. Matter Mater. Phys.* **2011**, *83* (7), 1–7.

(66) Asari, Y.; Suwa, Y.; Hamada, T. Formation and diffusion of vacancy-polaron complex in olivine-type $LiMnPO_4$ and $LiFePO_4$. *Phys. Rev. B* **2011**, *84* (13), 134113.

(67) Yamada, A.; Chung, S.-C. Crystal Chemistry of the Olivine-Type $Li(Mn_yFe_{1-y})PO_4$ and $(Mn_yFe_{1-y})PO_4$ as Possible 4 V Cathode Materials for Lithium Batteries. *J. Electrochem. Soc.* **2001**, *148* (8), A960–A967.

(68) Di Lecce, D.; Brutti, S.; Panero, S.; Hassoun, J. A new Sn-C/$LiFe_{0.1}Co_{0.9}PO_4$ full lithium-ion cell with ionic liquid-based electrolyte. *Mater. Lett.* **2015**, *139*, 329–332.

(69) Ludwig, J.; Marino, C.; Haering, D.; Stinner, C.; Gasteiger, H. A.; Nilges, T. Morphology-controlled microwave-assisted solvothermal synthesis of high-performance $LiCoPO_4$ as a high-voltage cathode material for Li-ion batteries. *J. Power Sources* **2017**, *342*, 214–223.

(70) Muraliganth, T.; Manthiram, A. Understanding the Shifts in the Redox Potentials of Olivine $LiM_{1-y}M_yPO_4$ (M = Fe, Mn, Co, and Mg) Solid Solution Cathodes. *J. Phys. Chem. C* **2010**, *114* (36), 15530–15540.

(71) Elia, G. A.; Ulissi, U.; Jeong, S.; Passerini, S.; Hassoun, J. Exceptional long-life performance of lithium-ion batteries using ionic liquid-based electrolytes. *Energy Environ. Sci.* **2016**, *9* (10), 3210–3220.

(72) Xing, L. Y.; Hu, M.; Tang, Q.; Wei, J. P.; Qin, X.; Zhou, Z. Improved cyclic performances of $LiCoPO_4$/C cathode materials for high-cell-potential lithium-ion batteries with thiophene as an electrolyte additive. *Electrochim. Acta* **2012**, *59*, 172–178.

(73) Sharabi, R.; Markevich, E.; Fridman, K.; Gershinsky, G.; Salitra, G.; Aurbach, D.; Semrau, G.; Schmidt, M. a.; Schall, N.; Bruenig, C. Electrolyte solution for the improved cycling performance of $LiCoPO_4$/C composite cathodes. *Electrochem. commun.* **2013**, *28*, 20–23.

(74) Markevich, E.; Salitra, G.; Fridman, K.; Sharabi, R.; Gershinsky, G.; Garsuch, A.; Semrau, G.; Schmidt, M. A.; Aurbach, D. Fluoroethylene Carbonate as an Important Component in Electrolyte Solutions for High-Voltage Lithium Batteries: Role of Surface Chemistry on the Cathode. *Langmuir* **2014**, *30* (25), 7414–7424.

(75) Hanafusa, R.; Oka, Y.; Nakamura, T. Electrochemical and Magnetic Studies of Li-Deficient $Li_{1-x}Co_{1-x}Fe_xPO_4$ Olivine Cathode Compounds. *J. Electrochem. Soc.* **2014**, *162* (2), A3045–A3051.

(76) Laszczynski, N.; Birrozzi, A.; Maranski, K.; Copley, M.; Schuster, M. E.; Passerini, S. Effect of coatings on the green electrode processing and cycling behaviour of $LiCoPO_4$. *J. Mater. Chem. A* **2016**, *4* (43), 17121–17128.

(77) Maeyoshi, Y.; Miyamoto, S.; Noda, Y.; Munakata, H.; Kanamura, K. Effect of organic

additives on characteristics of carbon-coated $LiCoPO_4$ synthesized by hydrothermal method. *J. Power Sources* **2017**, *337*, 92–99.

(78) Liu, D.; Zhu, W.; Kim, C.; Cho, M.; Guerfi, A.; Delp, S. A.; Allen, J. L.; Jow, T. R.; Zaghib, K. High-energy lithium-ion battery using substituted $LiCoPO_4$: From coin type to 1 Ah cell. *J. Power Sources* **2018**, *388*, 52–56.

(79) Benítez, A.; Caballero, Á.; Rodríguez-Castellón, E.; Morales, J.; Hassoun, J. The Role of Current Collector in Enabling the High Performance of Li/S Battery. *ChemistrySelect* **2018**, *3* (37), 10371–10377.

(80) Sharabi, R.; Markevich, E.; Borgel, V.; Salitra, G.; Aurbach, D.; Semrau, G.; Schmidt, M. A.; Schall, N.; Stinner, C. Significantly improved cycling performance of $LiCoPO_4$ cathodes. *Electrochem. commun.* **2011**, *13* (8), 800–802.

Table of Contents Image

Manganese and iron substitution for cobalt in the high-energy $LiCoPO_4$ cathode have opposite effects on the lithium cell behavior.